Self-demodulation of amplitude- and frequency-modulated pulses in a thermoviscous fluid

Michalakis A. Averkiou, Yang-Sub Lee, and Mark F. Hamilton
Department of Mechanical Engineering, The University of Texas at Austin, Austin, Texas 78712-1063

(Received 21 January 1993; accepted for publication 15 June 1993)

The self-demodulation of pulsed sound beams in a thermoviscous fluid is investigated experimentally and theoretically. Experiments were performed in glycerin at megahertz frequencies with amplitude- and frequency-modulated pulses. The theory is based on the Khokhlov–Zabolotskaya–Kuznetsov (KZK) nonlinear parabolic wave equation. Numerical results were obtained from an algorithm that solves the KZK equation in the time domain [Y.-S. Lee and M. F. Hamilton, *Ultrasonics International 91 Conference Proceedings* (Butterworth–Heinemann, Oxford, 1991), pp. 177–180]. A quasilinear analytic solution, which describes the main features of the waveform at all axial locations, is developed in the limit of strong absorption. Theory and experiment are in good agreement throughout the near- and far fields.

PACS numbers: 43.25.Lj

INTRODUCTION

The term "self-demodulation," which was coined in the 1960s by Berktay,[1] refers to the nonlinear generation of a low-frequency signal by a pulsed, high-frequency sound beam. Berktay derived a far-field axial solution for the demodulated waveform that is valid when the following conditions are satisfied: The amplitude modulation of the carrier wave (i.e., the pulse envelope) varies slowly relative to the center frequency of the pulse; the absorption length at the center frequency does not exceed the Rayleigh distance at that frequency; and the process is weakly nonlinear (no shock formation). The demodulated waveform predicted by Berktay is proportional to the second derivative of the square of the pulse envelope function, and it was first confirmed experimentally by Moffett *et al.*[2,3] Berktay's result is an extension of Westervelt's solution for the parametric array.[4] Limitations of Berktay's model, particularly with respect to the effects of absorption and pulse duration, are discussed by Frøysa.[5] Although many papers have been written on the subject of self-demodulation (see Refs. 5 and 6 for reviews of relevant literature), comparison of theory and experiment has been made only for the far-field axial waveform.

One purpose of the present paper is to demonstrate that the Khokhlov–Zabolotskaya–Kuznetsov (KZK) parabolic nonlinear wave equation[7] accurately describes the entire process of self-demodulation throughout the near field and into the far field, both on and off the axis of the beam. Numerical solutions of the KZK equation are obtained from a time-domain algorithm developed previously by two of the authors.[8] The numerical solutions are compared with results from experiments performed in glycerin at megahertz frequencies. Both amplitude- and frequency-modulated pulses are considered.

Another purpose of the paper is to present a quasilinear analytic solution that describes the complete evolution of the axial waveform. The second-order solution for the demodulated waveform accounts for the amplitude modulation considered by Berktay, the frequency modulation introduced by Gurbatov *et al.*,[9] and the effect of absorption as included by Cervenka and Alais.[6] The complete axial solution is obtained by combining the second-order solution with the results developed by Frøysa *et al.*[10] for the primary beam. Whereas the individual elements of the complete solution have been introduced previously by others, their combination provides a new result that is in excellent agreement with the numerical solution[8] for weak nonlinearity (Gol'dberg numbers less than unity) and strong absorption (absorption lengths less than the Rayleigh distance).

I. GOVERNING EQUATION AND SOURCE CONDITION

Our theoretical predictions are based on the KZK equation:[7]

$$\frac{\partial^2 p}{\partial z\,\partial t'}=\frac{c_0}{2}\nabla_r^2 p+\frac{\delta}{2c_0^3}\frac{\partial^3 p}{\partial t'^3}+\frac{\beta}{2\rho_0 c_0^3}\frac{\partial^2 p^2}{\partial t'^2}, \tag{1}$$

where p is the sound pressure, z is the coordinate along the axis of the beam, $\nabla_r^2=\partial^2/\partial r^2+r^{-1}(\partial/\partial r)$, r is the transverse radial coordinate (the sound beam is assumed to be axisymmetric), $t'=t-z/c_0$ is the retarded time, and c_0 is the sound speed. The first term on the right-hand side of Eq. (1) accounts for diffraction, the second term accounts for thermoviscous attenuation (δ is the diffusivity of sound[11]), and the third term accounts for quadratic nonlinearity of the fluid (β is the coefficient of nonlinearity and ρ_0 is the ambient density of the fluid).

The source is assumed to be a circular piston of radius a, for which the prescribed source condition is

$$p=p_0 f(t)H(a-r)\quad \text{at } z=0, \tag{2}$$

where p_0 is the characteristic source pressure, $f(t)$ is the time dependence, and H is the unit step function defined by $H(x)=0$ for $x<0$ and $H(x)=1$ for $x\geqslant 0$. Amplitude and frequency modulation of a carrier wave at frequency ω_0 are taken into account by writing

 0001-4966/93/94(5)/2876/8/$6.00

$$f(t)=E(t)\sin[\omega_0 t+\phi(t)], \tag{3}$$

where the envelope $E(t)$ and phase $\phi(t)$ are slowly varying functions of time in comparison with $\sin \omega_0 t$. The instantaneous angular frequency of the carrier wave is

$$\Omega(t)=\omega_0+\frac{d\phi}{dt}. \tag{4}$$

The source condition described by Eqs. (2) and (3) applies to all numerical and analytical results presented below.

II. NUMERICAL SOLUTION

The numerical solution is based on a dimensionless, transformed, and integrated form of Eq. (1):

$$\frac{\partial P}{\partial \sigma}=\frac{1}{4(1+\sigma)^2}\int_{-\infty}^{\tau}(\nabla_\rho^2 P)d\tau'+A\frac{\partial^2 P}{\partial \tau^2}+\frac{NP}{(1+\sigma)}\frac{\partial P}{\partial \tau}. \tag{5}$$

The dimensionless variables are defined by the following transformation, which facilitates calculations in the far field:[12]

$$P=(1+\sigma)(p/p_0), \quad \sigma=z/z_0,$$

$$\rho=(r/a)/(1+\sigma), \quad \tau=\omega_0 t'-(r/a)^2/(1+\sigma),$$

where $z_0=\omega_0 a^2/2c_0$ is the Rayleigh distance at a characteristic frequency ω_0. The following two parameters indicate the relative importance of the terms on the right-hand side of Eq. (5):

$$A=\alpha_0 z_0, \quad N=z_0/\bar{z},$$

where $\alpha_0=\delta\omega_0^2/2c_0^3$ is the thermoviscous attenuation coefficient and $\bar{z}=\rho_0 c_0^3/\beta\omega_0 p_0$ is the plane wave shock formation distance, each at frequency ω_0. A useful auxiliary parameter is the Gol'dberg number

$$\Gamma=N/A=(\alpha_0\bar{z})^{-1},$$

which appears in the quasilinear solution developed in Sec. III.

Equation (5) is solved numerically in the time domain via the algorithm described in Ref. 8. The pressure field $P(\rho,\sigma,\tau)$ is discretized in space and time, and Eq. (5) is integrated numerically term by term to advance the field through each incremental step from σ to $\sigma+\Delta\sigma$. Specifically, for a given pressure distribution in a plane at an arbitrary distance σ from the source plane, diffraction is taken into account by solving the equation

$$\frac{\partial P}{\partial \sigma}=\frac{1}{4(1+\sigma)^2}\int_{-\infty}^{\tau}(\nabla_\rho^2 P)d\tau' \tag{6}$$

with implicit finite difference methods. The solution of Eq. (6), now in the plane at $\sigma+\Delta\sigma$, is taken to be the new field back at σ, and absorption is taken into account by solving the equation

$$\frac{\partial P}{\partial \sigma}=A\frac{\partial^2 P}{\partial \tau^2}, \tag{7}$$

again with implicit finite difference methods. The solution in the plane at $\sigma+\Delta\sigma$ now includes the effects of both diffraction and absorption. A third sweep from σ to $\sigma+\Delta\sigma$ includes nonlinearity by implementing the relation

$$P(\rho,\sigma+\Delta\sigma,\tau)=P\left[\rho,\sigma,\tau+NP\ln\left(1+\frac{\Delta\sigma}{1+\sigma}\right)\right], \tag{8}$$

which is an exact solution of the equation

$$\frac{\partial P}{\partial \sigma}=\frac{NP}{(1+\sigma)}\frac{\partial P}{\partial \tau}. \tag{9}$$

The three successive sweeps over the incremental step $\Delta\sigma$ thus yield a solution in the plane at $\sigma+\Delta\sigma$ which contains the combined effects of diffraction, absorption, and nonlinearity.

The same procedure is repeated over each successive incremental step in the σ direction. Implicit backward finite difference (IBFD) methods are used to solve Eqs. (6) and (7) for the first 100 steps, and Crank–Nicolson finite difference (CNFD) methods are used throughout the remainder of the field. Typical step sizes used to generate the numerical results in Sec. V were $\Delta\sigma=10^{-3}\times(1+\sigma)^2$ for the IBFD methods and $\Delta\sigma=3.5\times10^{-3}(1+\sigma)^2$ for the CNFD methods, with $\Delta\rho\simeq0.03$ and $\Delta\tau\simeq0.2$. The implementation of the IBFD and CNFD methods with the indicated spatial step sizes is patterned after numerical algorithms for solving Fourier series expansions of Eq. (5), which are reviewed by Naze Tjøtta *et al.*[13] Additional details of the present algorithm will appear in a future paper.

III. QUASILINEAR AXIAL SOLUTION

As an alternative to the numerical solution described in the previous section, an analytic solution can be developed for the axial field. The method of successive approximations is used to obtain a solution of the form

$$p=p_1+p_2, \tag{10}$$

where p_1 and p_2 are the primary and secondary pressure fields, respectively, which satisfy the following equations:

$$\frac{\partial^2 p_1}{\partial z\,\partial t'}-\frac{c_0}{2}\nabla_r^2 p_1-\frac{\delta}{2c_0^3}\frac{\partial^3 p_1}{\partial t'^3}=0, \tag{11}$$

$$\frac{\partial^2 p_2}{\partial z\,\partial t'}-\frac{c_0}{2}\nabla_r^2 p_2-\frac{\delta}{2c_0^3}\frac{\partial^3 p_2}{\partial t'^3}=\frac{\beta}{2\rho_0 c_0^3}\frac{\partial^2 p_1^2}{\partial t'^2}. \tag{12}$$

Equations (10)–(12) shall be used to obtain a quasilinear solution for the complete axial waveform, subject to the source condition given by Eqs. (2) and (3). It is assumed that thermoviscous absorption terminates the nonlinear interaction region within the near field of the primary beam ($A \gtrsim 1$), and that finite-amplitude effects are relatively weak ($\Gamma \lesssim 1$).

As discussed by Frøysa *et al.*,[10] Eq. (11) can be solved by performing a temporal convolution of the lossless solution (obtained with $\delta=0$) with the dissipation function

$$D(z,t)=(c_0^3/2\pi\delta z)^{1/2}\exp(-c_0^3 t^2/2\delta z). \tag{13}$$

For the source condition in Eq. (2), the axial solution thus becomes

$$p_1/p_0=[f(t')-f(t'-a^2/2c_0z)]*D(z,t'), \quad (14)$$

where the asterisk indicates convolution with respect to t'. Because of the parabolic approximation inherent in the KZK equation, the validity of Eq. (14) is restricted at a given frequency ω_0 to distances of order[14,15] $z/a \gtrsim (\omega_0 a/c_0)^{1/3}$. All measurements reported in Sec. V satisfy this condition.

The convolution in Eq. (14) can be performed analytically for $E(t)$ a Gaussian envelope function, and for $\phi(t)$ a quadratic function of time [i.e., for which the instantaneous frequency $\Omega(t)$ varies linearly with time]. The analytic result for the corresponding plane wave case, with $\phi=$const (no frequency modulation), is discussed in Ref. 10.

To construct a solution for p_2, we begin with the main assumptions of Westervelt and Berktay, i.e., that absorption terminates the nonlinear interaction within the near field of the primary beam ($A \gtrsim 1$). An exponentially attenuated, collimated plane wave then provides a reasonable model for the virtual source distribution that generates the secondary pressure field. It is further assumed that the envelope E and phase modulation ϕ vary sufficiently slowly that thermoviscous absorption can be represented by exponential attenuation that acts locally according to the instantaneous frequency Ω of the carrier wave,[9] i.e.,

$$p_1(r,z,t') \simeq p_0 e^{-\alpha(t')z} E(t') \sin[\omega_0 t' + \phi(t')] H(a-r), \quad (15)$$

where

$$\alpha(t') = [\Omega(t')/\omega_0]^2 \alpha_0 \quad (16)$$

is a time-dependent attenuation coefficient proportional to Ω^2.

We now construct an asymptotic solution for p_2 by first ignoring the effect of absorption on the demodulated waveform, and we set $\delta=0$ in Eq. (12). The resulting lossless axial solution, designated by $\hat{p}_2$, is given by the volume integral

$$\hat{p}_2=\frac{\beta}{2\rho_0 c_0^4}\frac{\partial^2}{\partial t'^2} \times \int_0^z \int_0^\infty p_1^2\left(r',z',t'-\frac{r'^2}{2c_0(z-z')}\right)\frac{r'\,dr'\,dz'}{z-z'}. \quad (17)$$

Since the main contributions to the integral occur close to the source ($z' \lesssim \alpha^{-1}$) and the beam is assumed to be perfectly collimated ($p_1=0$ for $r'>a$), Eq. (17) reduces in the far field (i.e., z large in comparison with both α^{-1} and $\omega_2 a^2/2c_0$, where the latter quantity is the Rayleigh distance corresponding to radiation at a characteristic secondary frequency ω_2) to

$$\hat{p}_2 \sim \frac{\beta}{2\rho_0 c_0^4 z}\frac{d^2}{dt'^2}\int_0^\infty \int_0^\infty p_1^2(r',z',t')r'\,dr'\,dz'. \quad (18)$$

The waveform described by the square of Eq. (15) contains localized energy spectra at frequencies $\omega \ll \omega_0$ and $\omega \simeq 2\omega_0$ because $\alpha(t')$, $E(t')$, and $\phi(t')$ are all slowly varying functions of time in comparison with $\sin \omega_0 t'$. At distances $z \gg \alpha_0^{-1}$, the nonlinearly generated components at frequencies $\omega \simeq 2\omega_0$ are far more strongly attenuated than the components at frequencies $\omega \ll \omega_0$. Retaining only the low-frequency components in the forcing function permits us to write

$$p_1^2 \simeq (p_0^2/2) e^{-2\alpha(t')z} E^2(t') H(a-r). \quad (19)$$

Substitution of Eq. (19) into Eq. (18) thus yields

$$\hat{p}_2 \sim \frac{\beta p_0^2 a^2}{16\rho_0 c_0^4 z}\frac{d^2}{dt'^2}\frac{E^2(t')}{\alpha(t')}. \quad (20)$$

For $\phi=$const (no frequency modulation) we have $\alpha=$const, and Eq. (20) reduces to the result obtained by Berktay.[1] For $E=$const (no amplitude modulation), the result obtained by Gurbatov *et al.*[9] is recovered.

The effect of attenuation on the demodulated waveform is now taken into account. The nonlinear interaction region of radius a and length α^{-1} constitutes a reasonably compact volume directly in front of the transducer. Cervenka and Alais[6] included the effect of attenuation as though the demodulated waveform were radiated directly by the transducer. Following the same approach, we include attenuation by performing a temporal convolution of Eq. (20) with the dissipation function from linear theory:

$$p_2 \sim \frac{\beta p_0^2 a^2}{16\rho_0 c_0^4 z}\left(\frac{d^2}{dt'^2}\frac{E^2(t')}{\alpha(t')}\right)*D(z,t'). \quad (21)$$

A complete solution for the axial waveform can be obtained by combining the solutions for the primary and secondary fields. For $A \gtrsim 1$ and $\Gamma \lesssim 1$, the amplitude of the secondary wave does not approach that of the primary wave until the demodulated waveform is far from the nonlinear interaction region, where p_2 is given by Eq. (21). Closer to (or within) the nonlinear interaction region [i.e., before Eq. (21) is valid], the primary wave p_1 provides the main contribution to the total acoustic pressure p. We therefore substitute Eqs. (14) and (21) into Eq. (10) to obtain the complete quasilinear axial solution

$$\frac{p}{p_0}=\left[f(t')-f\left(t'-\frac{a^2}{2c_0 z}\right) + \frac{\beta p_0 a^2}{16\rho_0 c_0^4 z}\frac{d^2}{dt'^2}\frac{E^2(t')}{\alpha(t')}\right]*D(z,t'). \quad (22)$$

For comparison with the experimental and numerical results presented below, it is convenient to rewrite Eq. (22) in terms of the dimensionless quantities introduced in Sec. II:

$$\frac{p}{p_0}=\left[f(\tau)-f(\tau-\sigma^{-1})+\frac{\Gamma}{8\sigma}\frac{d^2}{d\tau^2}\left(\frac{E(\tau)}{1+d\phi/d\tau}\right)^2\right] * \frac{\exp(-\tau^2/4A\sigma)}{\sqrt{4\pi A\sigma}}, \quad (23)$$

where $\tau=\omega_0 t'$ (because $r=0$), and the asterisk now indicates convolution with respect to τ. To assess the relative

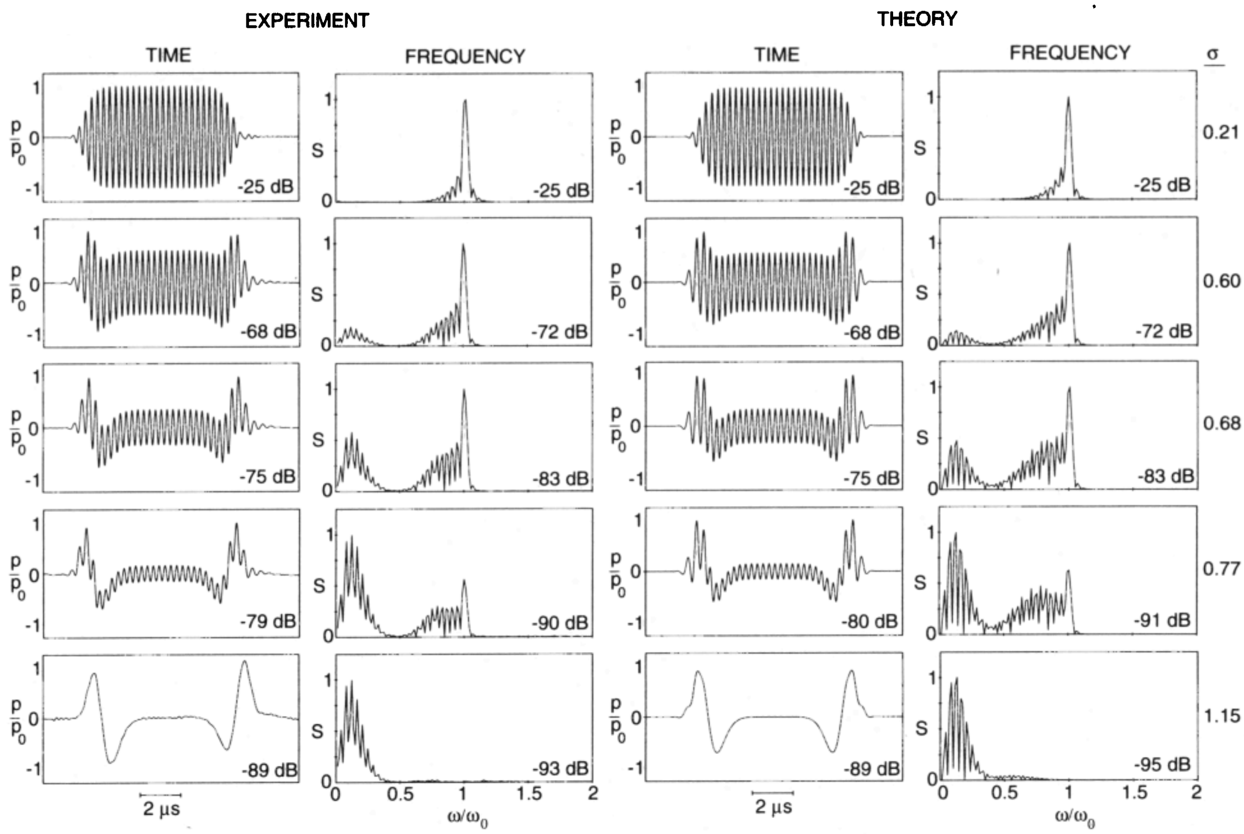

FIG. 1. Comparison of experiment and theory for the axial propagation of a 3.5-MHz pulse from $\sigma=0.21$ (first row) through $\sigma=1.15$ (last row). The theoretical predictions are obtained from numerical solutions of Eq. (5) with $\omega_0 T=50\pi$, $m=5$, $A=15$, and $N=1.6$ ($\Gamma=0.11$). Calculations based on Eq. (23) yield equally good agreement with experiment. Decibels indicate level relative to the corresponding source level.

magnitude of the demodulated waveform, let $E(t)=\sin\omega_e t$ and $\phi=\text{const}$. The resulting secondary pressure $p_-\equiv p_2$ contains the single frequency $\omega_-=2\omega_e$ and has magnitude

$$|p_-/p_0|=(\Gamma/16\sigma)(\omega_-/\omega_0)^2\exp[-(\omega_-/\omega_0)^2 A\sigma].$$

This result describes an absorption-limited parametric array[4] that produces the "difference frequency" $\omega_-=2\omega_e$.

IV. EXPERIMENT

Experiments were performed in a small tank filled with glycerin. Glycerin was chosen because it provides sufficiently large absorption at megahertz primary frequencies to permit investigation of the entire process of self-demodulation within distances on the order of tens of centimeters. In order for accurate comparisons to be made with predictions based on the KZK equation, the attenuation coefficient must depend on the square of the frequency. A quadratic frequency dependence was confirmed experimentally to within 2%. However, the tendency of glycerin to absorb moisture from the air caused the attenuation to vary slightly from day to day as a function of humidity (e.g., the attenuation at any given frequency would change by up to 10%, but the dependence on frequency remained quadratic). Nominal values for the density[16] and coefficient of nonlinearity[17] for glycerin are $\rho_0=1260\ \text{kg/m}^3$ and $\beta=5.4$, respectively. The value of the sound speed was found experimentally to be $c_0=1920$ m/s.

Our sound source was a Panametrics piezoelectric transducer with radius $a=0.64$ cm. The source was excited by signals produced with a LeCroy 9112 arbitrary function generator (50-MHz digitization rate, 12-bit amplitude resolution), which was programmed to generate waveforms defined by Eq. (3) with center frequency $f_0=\omega_0/2\pi=3.5$ MHz. The Rayleigh distance at this frequency was $z_0=23$ cm, and thermoviscous attenuation introduced losses of approximately 6 dB/cm. Envelope functions were defined by

$$E(t)=\exp[-(2t/T)^{2m}], \tag{24}$$

where T is the nominal duration of the pulse, which includes approximately $\omega_0 T/2\pi$ cycles at frequency ω_0, and the integer m determines the rise and decay time of the envelope. A Gaussian envelope is produced with $m=1$, and the rise time decreases as m increases, with a perfect rectangular envelope obtained with $m=\infty$. A characteristic rise time t_r may be defined by setting $|dE/dt|=t_r^{-1}$ at $t=\pm T/2$, which yields $t_r=(e/4m)T$. The receiving transducer was a Marconi bilaminar membrane hydrophone with an active element of diameter 1 mm and a response that was flat to within 0.5 dB over the frequency range of interest. The received signals were recorded and averaged with a Sony/Tektronix RTD 710 digitizer (200 MHz, 10 bits).

We encountered one particular experimental difficulty worth mentioning. Some measured waveforms that were

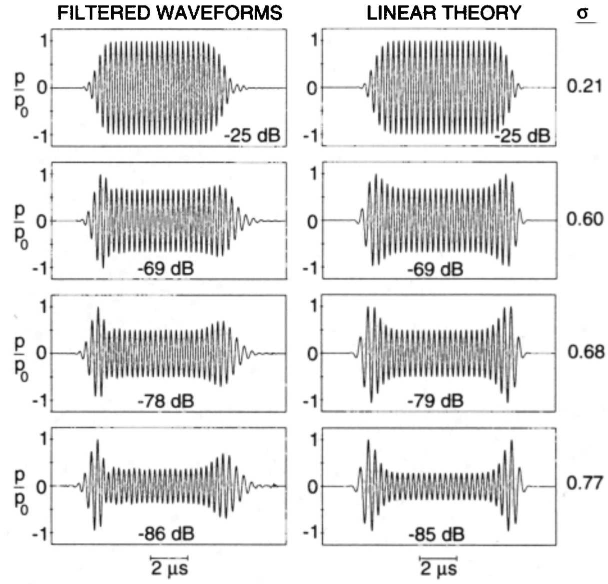

FIG. 2. Comparison of waveforms obtained by high-pass filtering (above approximately $\omega_0/2$) selected measured waveforms in the first column of Fig. 1 (left column above), with linear theory based on Eq. (14) (right column). Decibels indicate level relative to the corresponding source level.

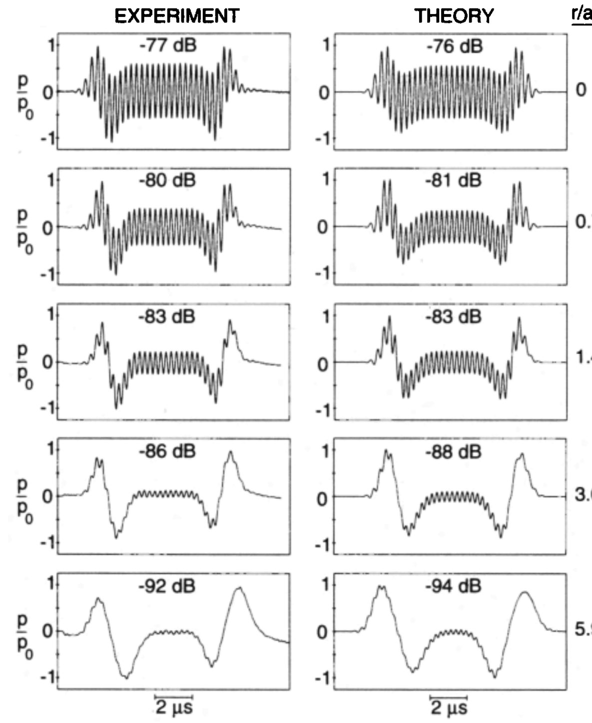

FIG. 3. Comparison of measured and predicted waveforms across the beam at $\sigma=0.55$, from $r/a=0$ (on axis) to $r/a=6$. The theoretical predictions are obtained from numerical solutions of Eq. (5) for the same parameters as in Fig. 1. Decibels indicate level relative to the corresponding source level.

described by the second derivative of the square of the envelope function (in agreement with the Berktay result) had amplitudes substantially larger than those predicted by theory. This anomaly was attributed to quadratic source nonlinearity, as follows. A piezoelectric source exhibits strain in response to an applied voltage $E(t)\sin\omega_0 t$, and therefore quadratic source nonlinearity may produce a displacement waveform component in the fluid that is proportional to E^2. The effective source pressure is proportional to particle velocity, which is the time derivative of this displacement (dE^2/dt), and propagation of the axial pressure waveform into the far field introduces yet a second time derivative as a result of diffraction (which leads to d^2E^2/dt^2). Special care was therefore exercised to find a source transducer that responded with suitable linearity over the desired range of operation.

V. RESULTS

Shown in Fig. 1 are results for the propagation of the axial waveform produced by a pulsed source with center frequency $f_0=3.5$ MHz. The first two columns contain the measured waveforms $p(\tau)/p_0$ and frequency spectra $S(\omega/\omega_0)$, and the second two columns contain the corresponding theoretical predictions. Equation (24) with $\omega_0 T=50\pi$ and $m=5$ was used for both the theoretical calculations and the input to the signal generator. The values of A and N were measured directly, and then minor adjustments were made to optimize comparison with theory, as follows. First, A was adjusted to provide the proper attenuation rate for the primary wave (small variations in A produced large variations in the predicted waveforms), and then N was adjusted to match the amplitude of the demodulated waveform. The result of this process yielded $A=15$ and $N=1.6$ (and therefore $\Gamma=0.11$), which correspond to an attenuation coefficient $\alpha_0=64$ Np/m and an effective peak source pressure $p_0=0.51$ MPa (i.e., 231 dB *re*: 1 μPa). The frequency spectra in the second and fourth columns of Fig. 1 are normalized to yield maximum amplitudes of unity at the source. Decibels given in each figure indicate level relative to that at the source. Whereas the theoretical predictions shown in Fig. 1 are provided by the numerical solution of Eq. (5), practically indistinguishable results are given by Eq. (23). Direct comparison of the numerical and analytical solutions is postponed to the end of this section.

Figure 1 demonstrates that overall agreement between theory and experiment is very good. Note the absence of second harmonic generation, which supports assumptions made in the derivation of Eq. (23). The slight asymmetry in the measured waveforms, which is most noticeable at $\sigma=1.15$, appears to be caused by asymmetry in the transient response of the source transducer (e.g., due to ringing).

We now consider the first-order components of the waveforms shown in Fig. 1. The waveforms in the left column of Fig. 2 were obtained by filtering out the low-frequency components (below approximately $\omega/\omega_0=0.5$) in the measured waveforms in the first column of Fig. 1. Linear theory based on Eq. (14), with $m=5$ and $\omega_0 T=50\pi$ in Eq. (24), is presented in the right column of Fig. 2. Small signal transient effects due to the high absorption produce the amplitude and phase modulations

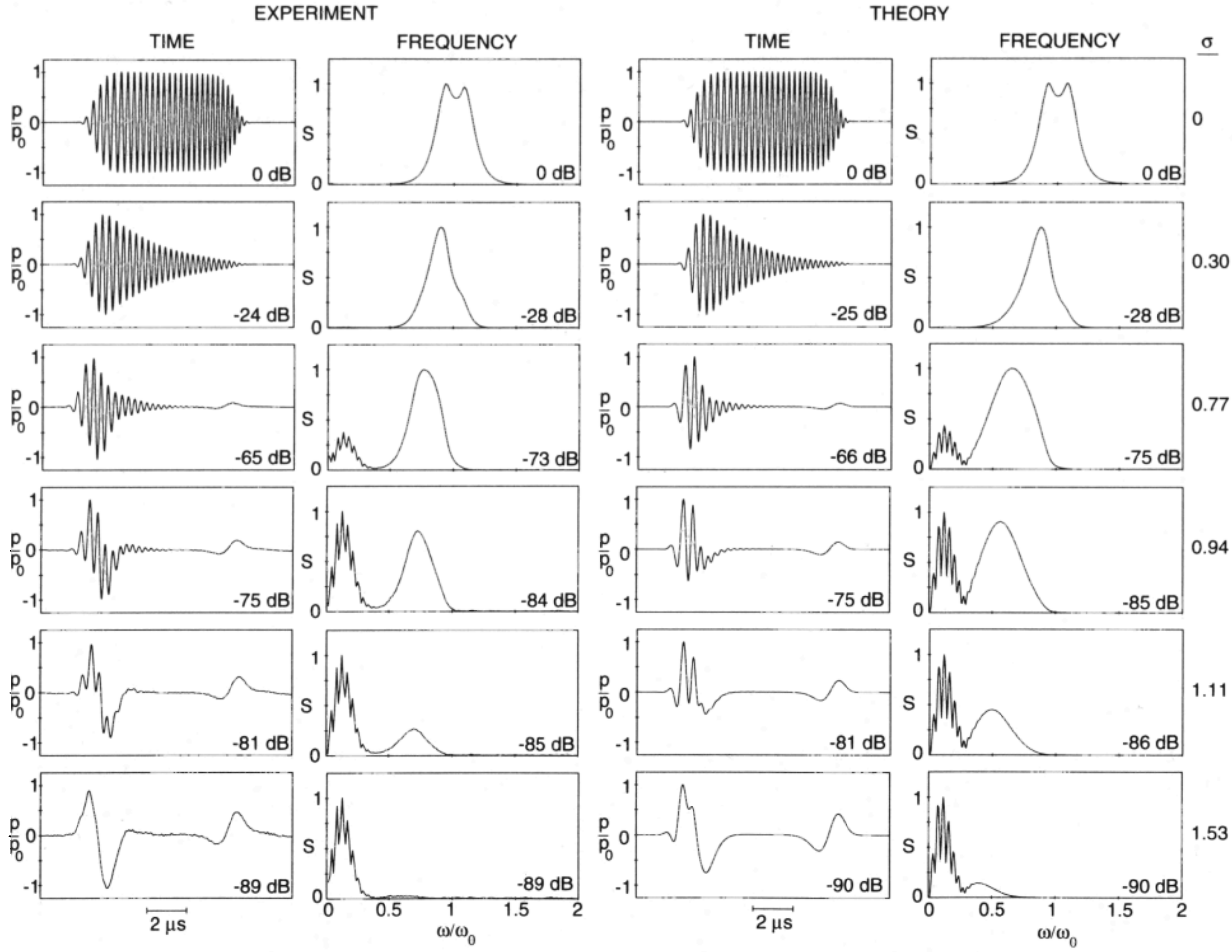

FIG. 4. Comparison of experiment and theory for the axial propagation of a frequency-modulated 3.5-MHz pulse from $\sigma=0$ (first row) through $\sigma=1.53$ (last row). The theoretical predictions are obtained from numerical solutions of Eq. (5) with $\phi=(\omega_0 t)^2/275\pi$, $\omega_0 T=50\pi$, $m=5$, $A=16$, and $N=1.6$ ($\Gamma=0.10$). Calculations based on Eq. (23) yield equally good agreement with experiment. Decibels indicate level relative to the corresponding source level.

(i.e., higher amplitudes and lower frequencies) at the beginnings and ends of the pulses. Similar effects were measured first by Moffett and Beyer[18] in an experiment designed to check the theoretical predictions of Blackstock.[19] Agreement between theory and experiment in Fig. 2 is somewhat better at the leading (left) end of each pulse than at the trailing end. The poorer agreement at the trailing end is consistent with the fact that effects of transducer ringing were more pronounced at that end. Also, the filtering process itself can introduce asymmetry. Comparison with Fig. 1 reveals that, at $\sigma=0.6$, the modulation of the waveform in Fig. 1 is due to both linear and nonlinear effects. Farther from the source, the dominant cause of modulation is the contribution from the secondary pressure p_2.

Measured and predicted waveforms both on and off axis, at $\sigma=0.55$, are compared in Fig. 3. The theory is obtained again from numerical solution of Eq. (5) [Eq. (23) applies only to the axial waveform], with the same parameter values used for Fig. 1. The higher directivity of the primary wave, compared with that of the demodulated waveform, leads to a relative suppression of the primary wave as the observation point is moved farther off axis. The measured waveforms in Figs. 1 and 3 reveal the same general features as those measured first by Moffett *et al.*[2,3]

Shown in Fig. 4 is the axial self-demodulation of a frequency-modulated tone burst with a center frequency of $f_0=3.5$ MHz and a phase modulation given by $\phi=(\omega_0 t)^2/275\pi$. The remaining parameters are $\omega_0 T=50\pi$, $m=5$, $A=16$, and $N=1.6$ ($\Gamma=0.10$). The instantaneous angular frequency of the tone is thus $\Omega/2\pi=f_0(1+4f_0 t/275)$, which increases linearly with time by approximately 50% over the duration of the pulse. The theory in Fig. 4 is obtained from the numerical solution of Eq. (5), although results obtained from Eq. (23) are virtually the same. We note that the experimental results shown for $\sigma=0$ correspond to the electrical input to the transducer and not the pressure in the fluid. At $\sigma=0.30$, absorption produces a greater effect at the trailing, high-frequency end of the pulse, and at $\sigma=0.77$, the nonlinear effect of self-demodulation is noticeable at the trailing end. At $\sigma=1.53$, the leading, low-frequency end of the pulse is nearly demodulated. The higher amplitude at the leading edge of the demodulated waveform corresponds to the lower primary frequency, and therefore longer nonlinear interaction region. We call attention to the fact that the predicted frequency spectra for the primary wave (i.e., for $\omega/\omega_0 \gtrsim 0.3$) are slightly broader than

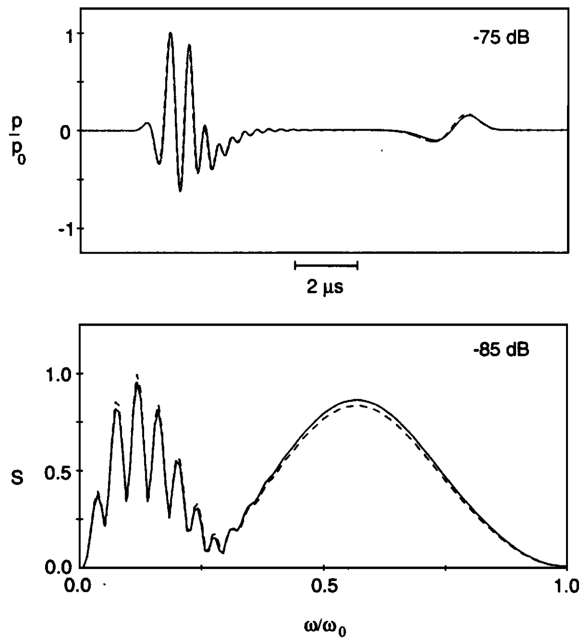

FIG. 5. Comparison of the theoretical prediction at $\sigma=0.94$ in Fig. 4, which was obtained by solving Eq. (5) numerically (solid lines above), with the prediction based on the quasilinear solution given by Eq. (23) (dashed lines).

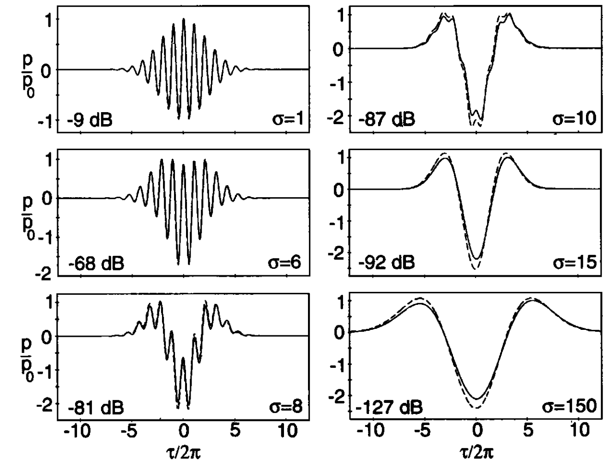

FIG. 6. Comparison of theoretical predictions for axial waveforms obtained by solving Eq. (5) numerically (solid lines) with predictions based on the quasilinear solution given by Eq. (23) (dashed lines), for $\omega_0 T=12\pi$, $m=1$, $A=1$, and $N=1$ $(\Gamma=1)$.

the corresponding measured spectra. The same is true, although somewhat less noticeable, in Fig. 1. These discrepancies are attributed, in part, to differences between the electrical input to the source transducer and the actual radiated waveform (recall the slight asymmetry of the measured waveforms in Figs. 1–3).

We have noted above that the quaslinear axial solution, Eq. (23), agrees very well with the numerical solutions that we compare with experiment in Figs. 1 and 4. The agreement is demonstrated in Fig. 5, where the quasilinear solution (dashed line) is compared with the numerical solution repeated from Fig. 4 for $\sigma=0.94$ (solid line).

Recall that Eq. (23) was derived for $A \gtrsim 1$ and $\Gamma \lesssim 1$, in addition to the restriction that the amplitude and frequency modulations be slowly varying functions. We therefore expect the agreement with the numerical solution to deteriorate when A and Γ have values of order unity, and for envelopes that vary more rapidly in comparison with the carrier frequency. In Fig. 6, we compare numerical and analytic solutions evaluated with the following parameter values: $A=1$, $\Gamma=1$, $m=1$, and $\omega_0 T=12\pi$. The numerical solution is again the solid line, and the quasilinear solution is the dashed line. Even for this limiting case, the approximate quasilinear solution is in good agreement with the complete numerical solution of the KZK equation. Slightly better agreement can be obtained, particularly in the second column, when finer discretization is used to obtain the finite difference solution (note that the maximum distance in Fig. 6 is two orders of magnitude greater than in the previous figures). Comparison of the waveforms at $\sigma=15$ and $\sigma=150$ demonstrates the effect of absorption on the demodulated waveform, which is discussed by Frøysa.[5]

Finally, the analytic and numerical solutions are compared in Fig. 7 for a case in which frequency modulation produces a strong effect on the demodulated waveform. We used the parameters $A=1$, $\Gamma=1$, $m=3$, and $\omega_0 T=50\pi$, and a phase modulation given by $\phi=-5\sin(\omega_0 t/25)$. The instantaneous frequency at $\sigma=0$ thus increases from $\Omega=0.8\omega_0$ in the center of the pulse to $\Omega \simeq 1.2\omega_0$ at either end. At $\sigma=4$, the main effect that can be seen is due to attenuation of the primary wave. The final demodulated waveform is achieved at $\sigma=24$, where the positive pressures at the ends of the waveform are due primarily to amplitude modulation, and the negative pressure in the middle is due primarily to frequency modulation. Again, the analytic and numerical solutions are in good agreement.

VI. SUMMARY

The self-demodulation of amplitude- and frequency-modulated pulses in a thermoviscous fluid has been inves-

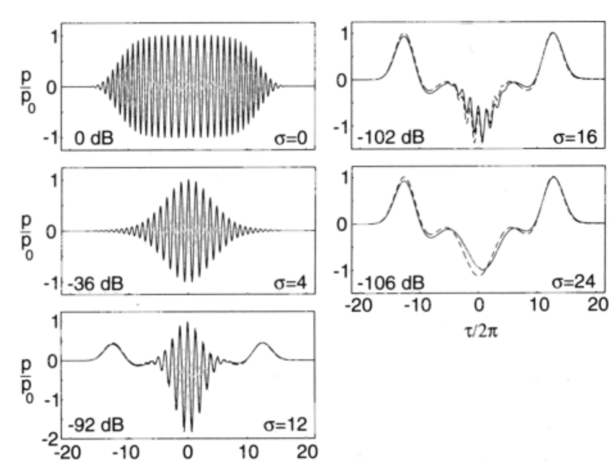

FIG. 7. Comparison of theoretical predictions for axial waveforms obtained by solving Eq. (5) numerically (solid lines) with predictions based on the quasilinear solution given by Eq. (23) (dashed lines), for $\omega_0 T=50\pi$, $m=3$, $A=1$, $N=1$ $(\Gamma=1)$, and $\phi=-5\sin(\omega_0 t/25)$.

tigated with both theory and experiment. Attention was devoted to the case in which absorption is sufficiently strong that the nonlinear interaction is relatively weak and restricted to the near field of the sound beam. A recently developed time-domain algorithm for solving the KZK equation was used to obtain numerical solutions. A quasilinear analytic solution for the entire axial field was developed and compared with both measurements and numerical results. The good agreement between theory and experiment demonstrates that the KZK equation and the analytic solution for the axial field provide accurate descriptions of the entire self-demodulation process.

ACKNOWLEDGMENTS

Discussions of this research with Professor Yu. A. Il'insky of Moscow State University are gratefully acknowledged. This work was supported by the David and Lucile Packard Foundation Fellowship for Science and Engineering, and by the Office of Naval Research. We also acknowledge the valuable preliminary support provided by the National Science Foundation and the Texas Advanced Research Program for the development of the Ultrasonics Laboratory in the Mechanical Engineering Department, where the experiments were performed. Computing resources were provided by The University of Texas System Center for High Performance Computing.

[1] H. O. Berktay, "Possible exploitation of non-linear acoustics in underwater transmitting applications," J. Sound Vib. **2**, 435–461 (1965).

[2] M. B. Moffett, P. J. Westervelt, and R. T. Beyer, "Large-amplitude pulse propagation—A transient effect," J. Acoust. Soc. Am. **47**, 1473–1474 (1970).

[3] M. B. Moffett, P. J. Westervelt, and R. T. Beyer, "Large-amplitude pulse propagation—A transient effect. II," J. Acoust. Soc. Am. **49**, 339–343 (1971).

[4] P. J. Westervelt, "Parametric end-fire array," J. Acoust. Soc. Am. **35**, 535–537 (1963).

[5] K.-E. Frøysa, "Weakly nonlinear propagation of a pulsed sound beam," in *Frontiers of Nonlinear Acoustics: 12th ISNA*, edited by M. F. Hamilton and D. T. Blackstock (Elsevier Applied Science, London, 1990), pp. 197–202.

[6] P. Cervenka and P. Alais, "Fourier formalism for describing nonlinear self-demodulation of a primary narrow ultrasonic beam," J. Acoust. Soc. Am. **88**, 473–481 (1990).

[7] N. S. Bakhvalov, Ya. M. Zhileikin, and E. A. Zabolotskaya, *Nonlinear Theory of Sound Beams* (American Institute of Physics, New York, 1987).

[8] Y.-S. Lee and M. F. Hamilton, "Nonlinear effects in pulsed sound beams," *Ultrasonics International 91 Conference Proceedings* (Butterworth–Heinemann, Oxford, 1991), pp. 177–180.

[9] S. N. Gurbatov, I. Yu. Demin, and A. N. Malakhov, "Influence of phase fluctuations on the characteristics of parametric arrays," Sov. Phys. Acoust. **26**, 217–220 (1980).

[10] K.-E. Frøysa, J. Naze Tjøtta, and S. Tjøtta, "Linear propagation of a pulsed sound beam from a plane or focusing source," J. Acoust. Soc. Am. **93**, 80–92 (1993).

[11] J. Lighthill, *Waves in Fluids* (Cambridge U.P., Cambridge, 1980), pp. 78–83.

[12] M. F. Hamilton, J. Naze Tjøtta, and S. Tjøtta, "Nonlinear effects in the farfield of a directive sound source," J. Acoust. Soc. Am. **78**, 202–216 (1985).

[13] J. Naze Tjøtta, S. Tjøtta, and E. H. Vefring, "Propagation and interaction of two collinear finite amplitude sound beams," J. Acoust. Soc. Am. **88**, 2859–2870 (1990).

[14] V. E. Kunitsyn and O. V. Rudenko, "Second-harmonic generation in the field of a piston radiator," Sov. Phys. Acoust. **24**, 310–313 (1978).

[15] J. Naze Tjøtta and S. Tjøtta, "An analytical model for the nearfield of a baffled piston transducer," J. Acoust. Soc. Am. **68**, 334–339 (1980).

[16] L. E. Kinsler, A. R. Frey, A. B. Coppens, and J. V. Sanders, *Fundamentals of Acoustics* (Wiley, New York, 1982), p. 462.

[17] R. T. Beyer, "Parameter of nonlinearity in fluids," J. Acoust. Soc. Am. **32**, 719–721 (1960).

[18] M. B. Moffett and R. T. Beyer, "Transient effects in the propagation of a sound pulse in a viscous liquid," J. Acoust. Soc. Am. **47**, 1241–1249 (1970).

[19] D. T. Blackstock, "Transient solution for sound radiated into a viscous fluid," J. Acoust. Soc. Am. **41**, 1312–1319 (1967).